第17回性能に基づく橋梁等の耐震設計に関する
シンポジウム講演論文集（2014年7月）

# EFFECTIVE STRESS ANALYSIS TO BEHAVIOR OF A STEEL PIPE SHEET PILE FOUNDATION IN THE SLOPE REVETMENT DURING LIQUEFACTION

Nguyen Thanh TRUNG[1], Osamu KIYOMIYA[2], Tongxiang AN[3] and Nguyen Thi Tuyet TRINH[4]

[1]Student member of JSCE, Doctoral student, Waseda University (〒169-8555 Tokyo, Shinjuku-ku, Okubo 3-4-1)

[2]Fellow member of JSCE, Professor, Waseda University (〒169-8555 Tokyo, Shinjuku-ku ,Okubo 3-4-1)

[3]Member of JSCE, A. Professor, Waseda University (〒169-8555 Tokyo, Shinjuku-ku, Okubo 3-4-1)

[4]Lecture, Doctor, University of Transport and Communication. (Dong Da, Hanoi, Viet Nam)

## 1. INTRODUCTION

The damages to the bridge foundation structure in the revetment along riverbanks and sea coasts caused by liquefaction have been observed during past earthquakes. The slope revetment is expected to be unstable, and lateral spreading of the ground may occur simultaneously with the loss of soil strength in the liquefaction layer. Therefore, the effect of the lateral pressure of the liquefaction layer on the foundation in the revetment must be investigated further. This study aims to investigate the dynamic behavior of vibration test models of a steel pipe sheet pile (SPSP) foundation by using the effective stress analysis (ESA). The vibration test conducted on a flat model and a slope model of 15° was a 1-G shaking table test with a scale of 1:60.

The effective stress analysis using a 2-D numerical modeling method was applied both the flat and slope model in this study. Recently, there have been a number of constitutive models to simulate soil response during liquefaction (e.g., Ishihara et al. 1985; Iai, 1991; Kimura et al., 1993; Tobita and Yoshida, 1995). It is called by a strain space multiple mechanism model and was widely used in seismic design practice in Japan. It was firstly suggested by Iai et al. (1991) named as a Multi Spring Model in the un-drained condition. Then, the model was also improved by Iai et al. (2010) names as a Glass Cocktail Model in the drained condition.

The comparison of responses between the effective stress analysis and vibration test also conducted in this study and the differences in the dynamic responses between the two models clearly illustrate the significant effect of the ground slope on the seismic behavior of the SPSP foundation. The FLIP program analysis was available.

## 2. EFFECTIVE STRESS ANALYSIS

The 2-D finite element method was used to simulate the behavior of foundation and soil-structure interaction. The effective stress analysis (ESA) technique was used both by the Multi-spring and Cocktail glass model. The FLIP program (developed by Port and Airport Research, Institute, Yokosuka, Japan) was used in this analysis.

### 2.1 Test models

Numerical models were simulated form vibration test models designed for both the flat and slope model. Detail of physical models and instrument arrangement are shown in the **Figs.1** and **2**

The pier in the model consists of four steel columns that are rigidly fixed together by a steel plate at the top with a mass of 60 kg. Each column has dimensions of 1.1 m height. The foundation is a caisson made of acrylic materials with a dimension of 49 cm width, 60.8 cm length, and 83.4 cm height. The cap at the top of the foundation is an acrylic plate that is 60.8 cm long, 49 cm wide, and 9.8 cm thick. The footing of the pier is constructed of steel.

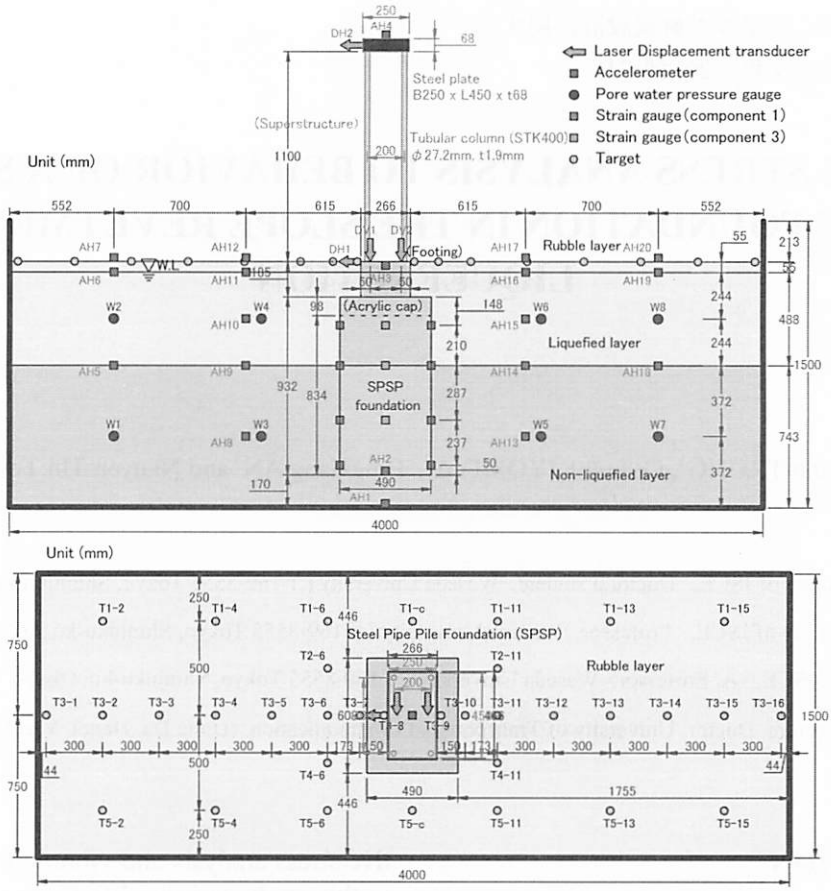


**Fig.1** General view of the flat model and transducers arrangement.

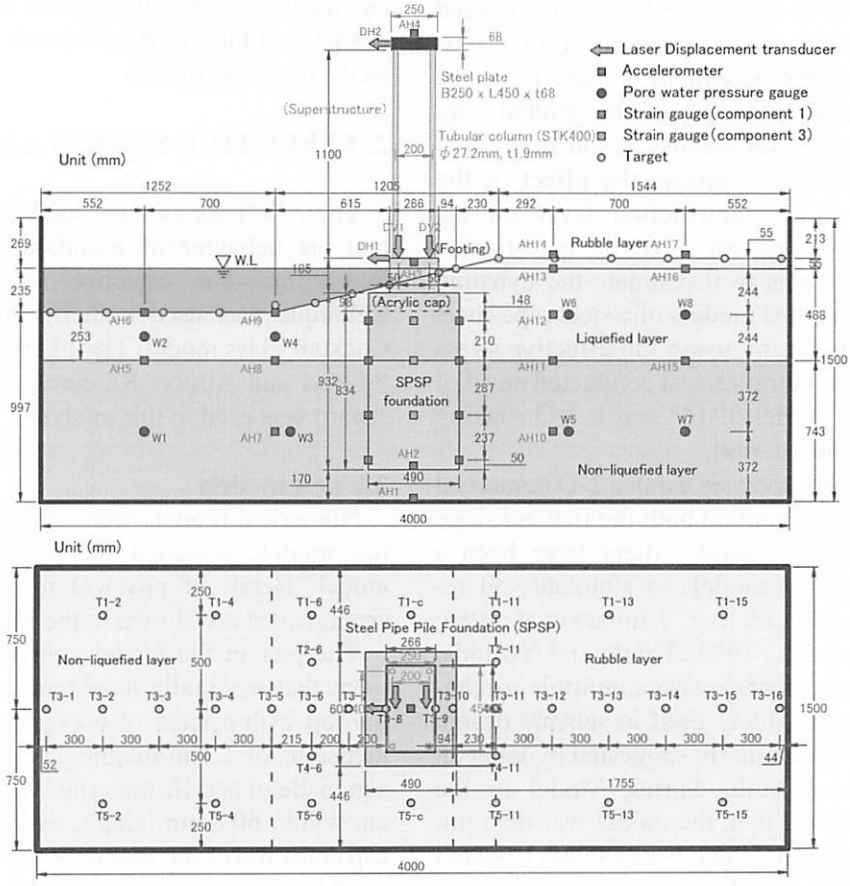


**Fig.2** General view of the slope model and transducers arrangement.

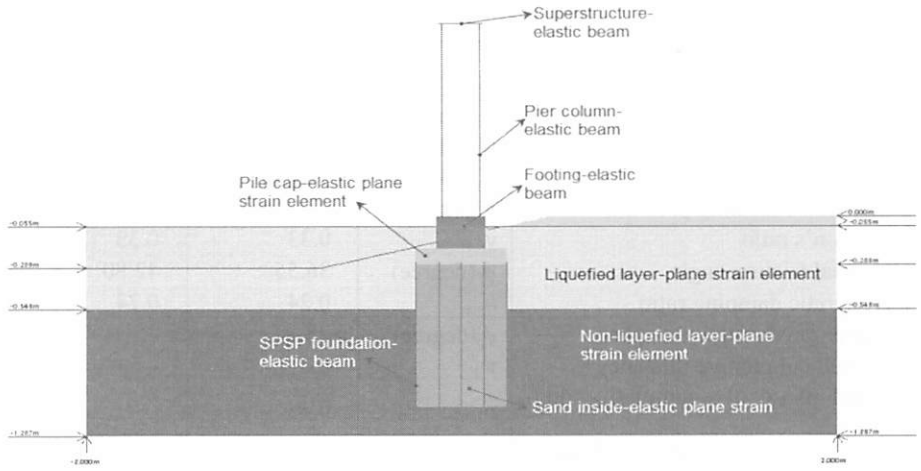


**Fig.3** Numerical slope model in Effective Stress Analysis (ESA).

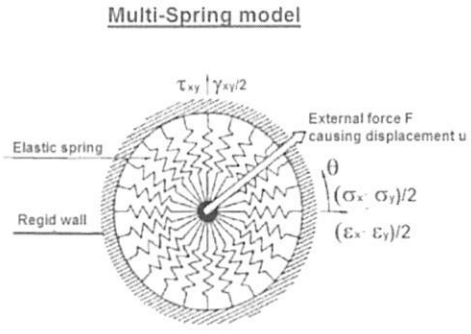


**Fig.4** Multi-spring model in effective stress analysis.

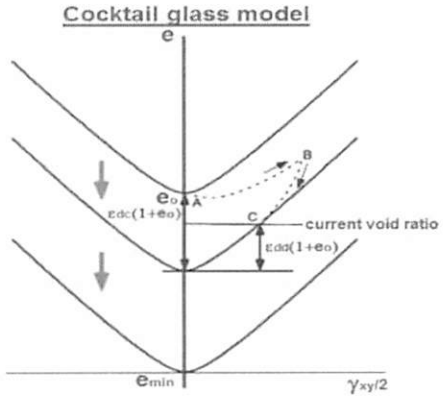


**Fig.5** Cocktail glass model in effective stress analysis.

The ground in the models consisted of a 48.8 cm liquefiable sand layer with a relative density of 50 % overlying a 74.3 cm non-liquefiable with a relative density of 90 % using Yamagata-sand No. 6 (D50 = 0.3 mm)

## 2.2. Numerical models

The boundary condition of pore water in ESA using the cocktail glass model was considered in the undrained conditions (no seepage) at side walls and bottom wall of the test vessel. The numerical model in the analysis is shown in **Fig.3**

The soil was modeled as plane strain elements using two liquefaction models of the loose sand. The first model is called a multi-spring model and is shown in **Fig.4**. The multi-spring model is a strain-space multiple-mechanism model. This model considers the effect of the rotation of the principal stress axes on the cyclic behavior of the sand. As shown in this figure, pore water pressure increases by calculation steps. The second model is a cocktail glass model improved from a strain-space multiple-mechanism model in the drained condition suggested by Iai *et al.*[17], as shown in **Fig.5**. There are two main assumptions in this model. First, the volumetric strain is decomposed in a dilative component and contractive component, as determined in Eq.(1). The dilative component affects the dissipation of pore water pressure in the steady state and the horizontal displacement response. The second is a relationship between relative velocity and coefficient of permeability determined in Eq.(2). This assumption influences the rate of pore water development and dissipation as follows:

$$\varepsilon_d = \varepsilon_d^c + \varepsilon_d^d \tag{1}$$

where $\varepsilon_d$ is the volumetric strain; $\varepsilon_d^c$ is the contractive component; and $\varepsilon_d^d$ is the dilative component.

The coefficient of permeability ($k$) suggested by Chapuis and Aubertin [19] for sand used in the cocktail glass model as follows:

$$k = C\frac{g}{\mu_w \rho_w}\frac{e^3}{S^2 D_R^2 (1+e)} \tag{2}$$

where $k$ is the coefficient of permeability; $C$ is a constant; $\mu_w$ is the dynamic viscosity of water; $\rho_w$ is the density of water; $D_R$ is the specific weight of sand; $S$ is the specific surface; and $e$ is the void ratio.

**Table 1** List of soil parameters.

| Parameter | | Symbol | Liquefaction layer | Non-liquefaction layer | Rubble layer |
|---|---|---|---|---|---|
| Parameters for deformation characteristics | Wet unit weight | $\rho$ (t/m$^3$) | 1.96 | 2.05 | 1.37 |
| | Initial shear modulus | $G_{ma}$ (kPa) | 3,866 | 21,788 | 2,993 |
| | Initial bulk modulus | $K_{ma}$( kPa ) | 10,083 | 56,819 | 7,805 |
| | Standard confining pressure | $\sigma_{ma}$'(kPa) | 2.27 | 6.85 | 0.28 |
| | Poisson's ratio | v | 0.33 | 0.33 | 0.33 |
| | Internal friction angle | $\phi_f$(degree) | 36.55 | 42.80 | 41.60 |
| | Hysteretic damping ratio | $h_{max}$ | 0.24 | 0.24 | 0.24 |
| Parameters for Muti-Spring model | Phase transformation angle | $\phi_p$(degree) | 28 | - | - |
| | Overall cumulative dilatancy | $w_1$ | 8.2 | - | - |
| | Initial phase of cumulative dilatancy | $p_1$ | 0.45 | - | - |
| | Final phase of cumulative dilatancy | $p_2$ | 1.07 | - | - |
| | Threshold limit for dilatancy | $c_1$ | 4.48 | - | - |
| | Ultimate limit of dilatancy | $S_1$ | 0.005 | - | - |
| Parameters for Cocktail glass model | Reduction factor of bulk modulus for liquefaction analysis | $r_K$ | 0.5 | - | - |
| | Power index of bulk modulus for liquefaction analysis | $l_K$ | 2 | - | - |
| | Parameter controlling dilative and contractive components | $r_{cd}$ | 0.5 | - | - |
| | Parameter controlling contractive component | $r^c_{cd}$ | 2 | - | - |
| | Parameter controlling initial phase of contractive component | $q_1$ | 1 | - | - |
| | Parameter controlling final phase of contractive component | $q_2$ | 1 | - | - |
| | Limit of contractive component | $\varepsilon^{cm}_d$ | 0.5 | - | - |
| | Small positive number to avoid zero confining pressure | $S_1$ | 0.005 | - | - |
| | Parameter controlling elastic range for contractive component | $c_1$ | 4.48 | - | - |

The liquefaction parameters of the soil layers are summarized in **Table 1.** The models were shaken with a base harmonic acceleration at a constant frequency of 10 Hz. The duration time was 2 s. The amplitude increased incrementally from 50 to 300 Gal, and one of the input stages is shown in **Fig.6**. The frequency and wave numbers of input ground motion was selected in the consideration of the subduction zone earthquakes (level 2 earthquake motion) and the similarity law

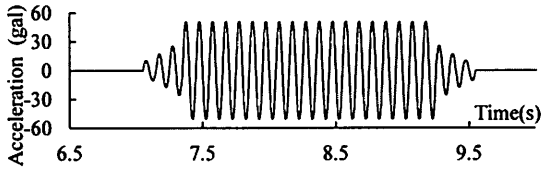


**Fig.6** Acceleration wave input at the base.

## 3. RESULT AND COMPARISON BETWEEN THE EFFECTIVE STRESS ANALYSIS AND THE EXPERIMENT

### 3.1. Behavior of ground

**a) Pore water pressure**

The time histories of the EPWP at points W4 in the near field and W8 in the far field of the experiment and ESA under the 300 Gal input ground motion are shown in **Figs.7** and **8** for the flat and slope models, respectively. The EPWP ratio did not exceed 0.8 and perfect liquefaction did not occur at 300 Gal. The results of the EPWP among the experiment, multi-spring model, and cocktail glass model are fairly different from each other. The liquefaction start time was almost identical for both methods, whereas the EPWP dissipation, maximum EPWP ratio, and vibration components differed considerably. The EPWP ratio gradually decreased after the vibration stopped in the experiment; this phenomenon can be explained using the cocktail glass model. The EPWP ratio was almost the same between the experiment and the cocktail model after 12 s. However, the generation and dissipation of EPWP in the model occurs very quickly during vibration time of 2 s. The cocktail glass model displayed a vibration component of the EPWP.

The EPWP ratio distribution of the ground under 300 Gal in the ESA multi-spring is shown in **Figs.9** and **10** for the flat and the slope models, respectively.

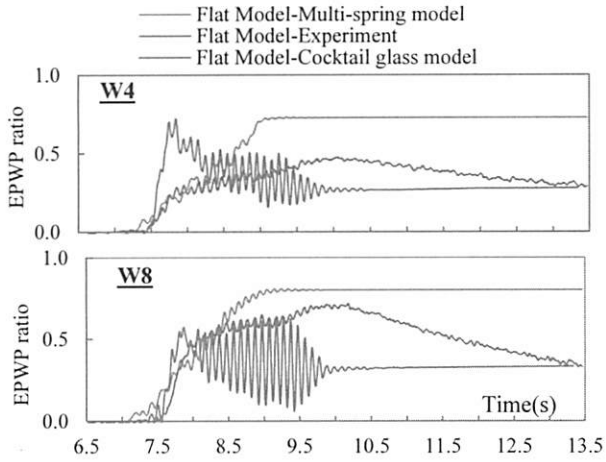


**Fig.7** Time history of EPWP ratio at W4 and W8 in the flat model under 300 Gal.

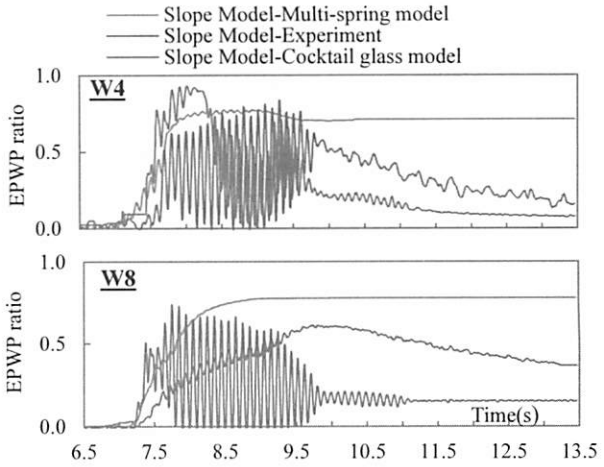


**Fig.8** Time history of EPWP ratio at W4 and W8 in the slope model under 300 Gal.

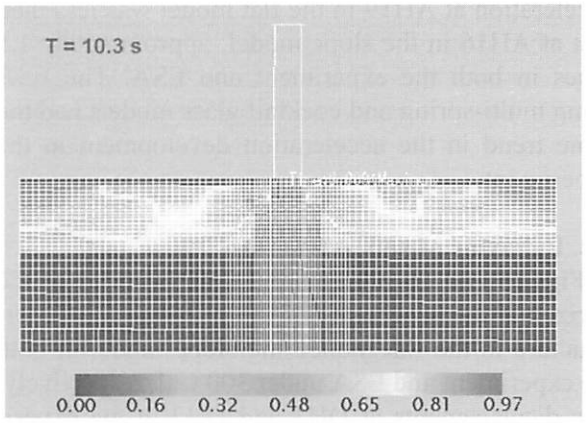


**Fig.9** EPWP ratio distribution in the flat model under 300 Gal in the ESA multi-spring.

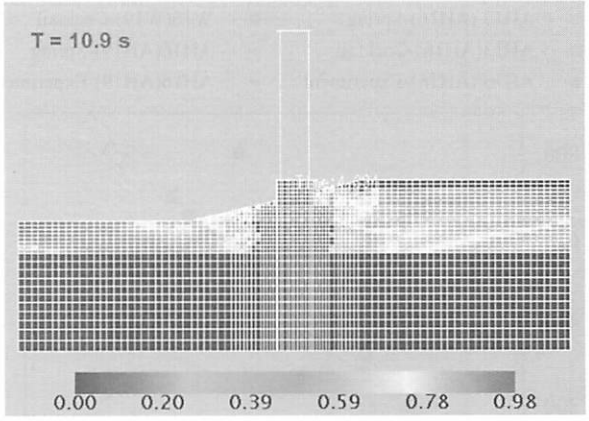


**Fig.10** EPWP ratio distribution in the slope model under 300 Gal in the ESA multi-spring.

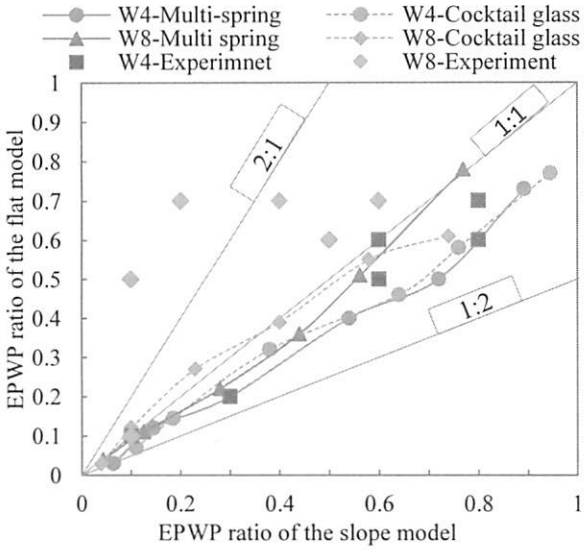


**Fig.11** Comparison of EPWP ratio at W4 and W8 between the flat and the slope models.

The EPWP ratio reached approximately 1.0 at the surface liquefied layer in both models after approximately 4 s. However, the EPWP was not uniform at the surface layer in the multi-spring model.

**Fig.11** compares the EPWP at W4 and W8 between the slope and flat models obtained by the experiment and ESA from 50 to 300 Gal. There are six red points in **Fig.11**, and their values gradually increase. The EPWP ratio of the slope model at W4 was 1.1÷1.25 times higher than that of the flat model in both the experiment and ESA. At W8 the EPWP ratios of ESA using both the multi-spring and cocktail models were nearly identical between the two models, but in the experiment, the ratios of the flat model were larger than those of the slope model.

**b) Horizontal acceleration**

**Fig.12** presents the time histories of the horizontal accelerations at points AH8 and AH19 in the flat model. In the non-liquefaction layer, the acceleration at AH8 of ESA corresponded well with that of the experiment, and the acceleration did not exhibit any amplitude variations during the shaking period. Meanwhile, the acceleration at far-field AH19 of the liquefaction layer varied significantly starting at 7.5 s, and this amplitude gradually decreased between 7.5 and 10 s, as shown in **Fig.12**.

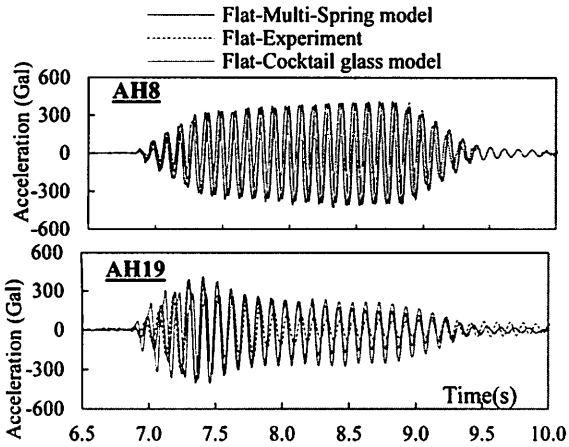


**Fig.12** Time history of acceleration at AH8, AH10 and AH19 in the flat model under 300 Gal.

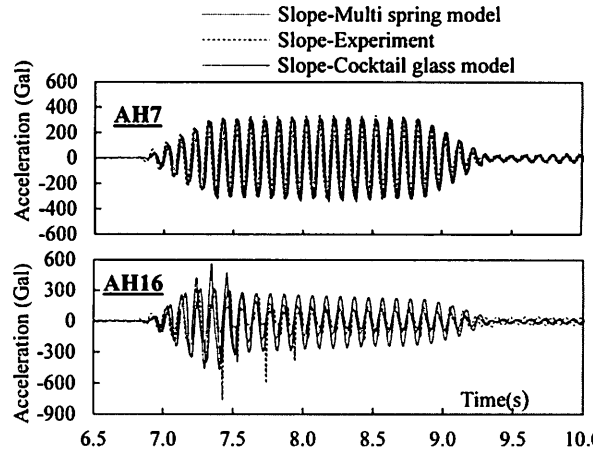


**Fig.13** Time history of acceleration at AH7, AH9 and AH16 in the slope model under 300 Gal.

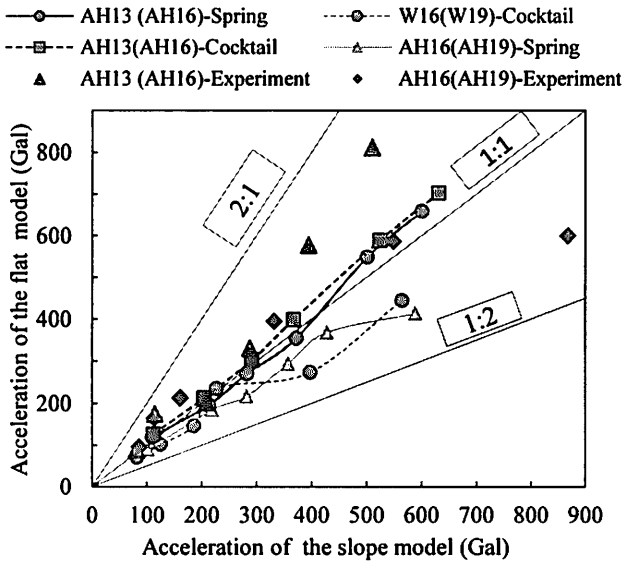


**Fig.14.** Comparison of acceleration at AH13, 16 in the flat model and AH16, 19 in the slope model.

The horizontal accelerations at points AH7 and AH16 in the slope model are shown in **Fig.13**. These points are at the same position, corresponding to points AH8 and AH19 in the flat model. Similar to the acceleration behavior in the flat model, the acceleration amplitude in the liquefaction layer at point AH16 decreased and did not appear in the non-liquefaction layer at AH7.

**Fig.14** presents a comparison of the horizontal accelerations at AH13, AH16 in the slope model and at AH16, AH19 in the flat model. The difference in the acceleration in the near field between AH13 in the slope model and AH16 in the flat model was minimal in the 50-150 Gal cases in both the experiment and ESA. However, the acceleration ratio steadily approached 2:1 in the 150-300 Gal cases. The acceleration at AH 13 in the flat model became approximately 1.5 times that of the slope model in the experiment under 300 Gal. In the far field, the acceleration at AH19 in the flat model was less than that at AH16 in the slope model, approximately 1.5 times in both the experiment and ESA. The ESA using multi-spring and cocktail glass models had the same trend in the acceleration development in the experiment.

### 3.2. Behavior of superstructure

**Figs.15** and **16** presents the time histories of the horizontal displacements of the pile cap and superstructure in the flat model and slope model in both the experiment and ESA under 300 Gal, respectively. The displacements at DH1 and DH2 in the experiment were larger than those in the ESA. The displacements in the ESA-cocktail-glass model were considerably smaller than the displacements in other cases. Figure 20 shows that the residual displacement calculated in the ESA and the difference of the maximum displacement between the ESA and experiment were rather large.

The maximum during shaking from 50 to 300 Gal are shown in **Fig.17**. There was a remarkable agreement between the experiment and ESA multi-spring for the maximum and residual displacement between 50 to 150 Gals; however, the displacements in the ESA multi-spring were considerably less than those in the experiment for the 150-300 Gal cases. Based on JRA-2002, the allowable displacement of 4.9 mm for the top of the foundation was calculated by multiplying the width of the foundation by 1%. Thus, when liquefaction occurred, the maximum horizontal displacements of the pile cap under the 300 Gal input ground motion was approximately 0.35 times less than the allowable displacement for the experiment, and 0.2 times less than that for the ESA multi-spring. Moreover, the maximum displacements in the ESA cocktail glass were approximately 2 times less than those in the experiment. The residual displacements were very small and not sig-

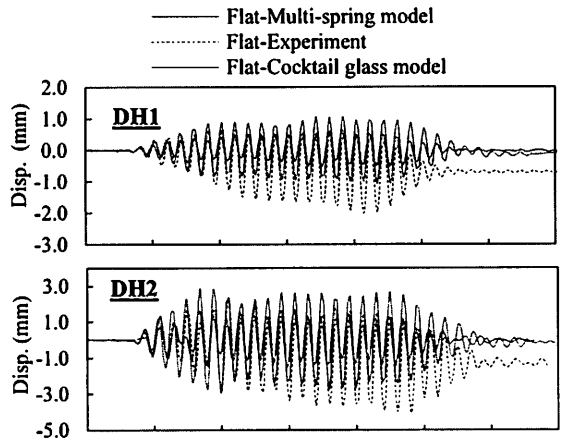


**Fig.15.** Displacement response at AH3 and AH4 in the flat model under 300 Gal

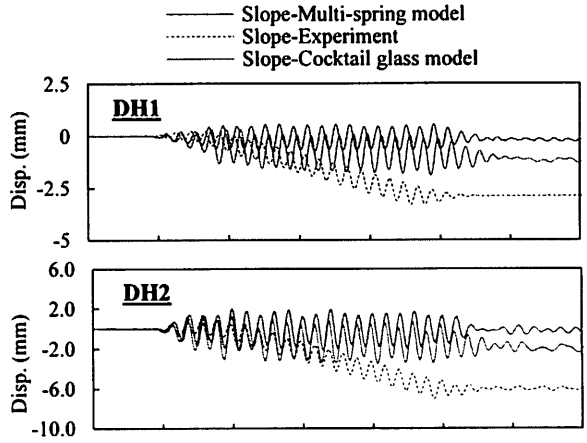


**Fig.16.** Displacement of superstructure and pile cap in the slope model under 300 Gal

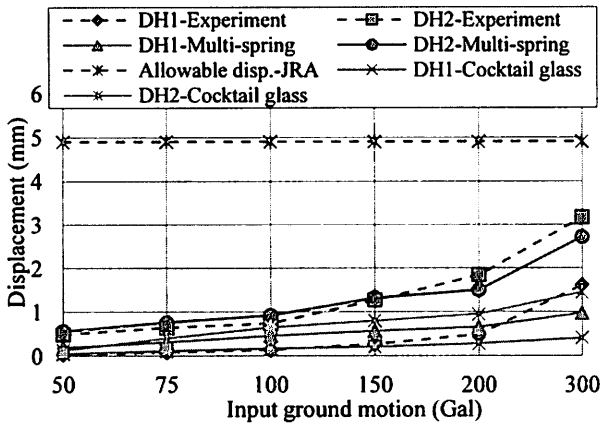


**Fig.17** Maximum horizontal displacement of the superstructure DH2 and pile cap DH1 in the flat model from 50 to 300 Gal.

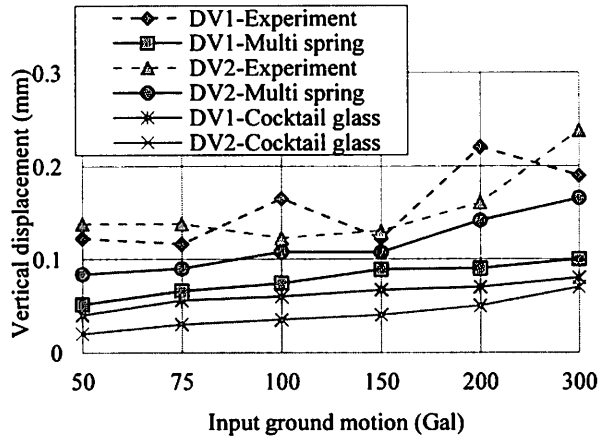


**Fig.18** Maximum vertical displacement of the pile cap at DV1 and DV2 in the flat model from 50 to 300 Gal.

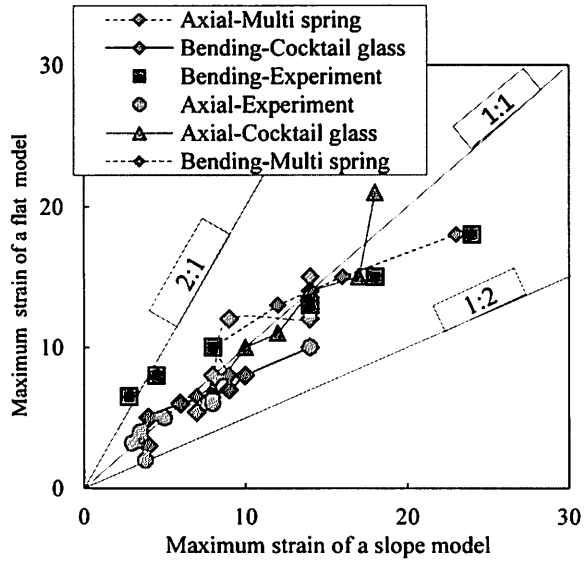


**Fig.19** Comparison of maximum strain along the front and back sides between the flat and slope models.

nificant during shaking.

**Fig.18** presents the maximum vertical displacements in the flat model during shaking under the 50-300 Gal input ground motion. There was a remarkable agreement between the experiment and ESA multi-spring. Moreover, there was a slight difference in the displacement value between DV1 and DV2 in both the experiment and ESA multi-spring. The settlement of the foundation in the flat model was almost even. The displacements in the ESA cocktail glass were much smaller than those of other cases.

### 3.3. Behavior of foundation

**Fig.19** presents a comparison of the maximum bending strain and axial strain of the pile foundation between the two models from 50 to 300 Gal in both the experiment and the ESA.

The maximum bending strain of the flat model in the experiment was almost larger than that of the slope model in the 50-150 Gal cases. However, when the liquefaction process was complete, the strain of the slope model became 1.5 times larger than that of the flat model in the 300 Gal case. For the ESA using both multi-spring and cocktail models from 50 to 200 Gal, the difference in the bending strain between the two models was minimal, and in the case of 300 Gal,

the strain of the slope model was approximately 1.3 times larger than that of the flat model. The result of the experiment also illustrates that the maximum axial strain in the slope model was approximately 1.5 times larger than that of the flat model. However, the axial strain difference in the ESA between the two models was small.

Moreover, ESA multi-spring had the same trend as that of the experiment; however, the strain in the slope model was slightly larger than that in the flat model.

## 4. CONCLUSIONS

The numerical analysis using the effective stress analysis was conducted on the both the flat and slope model of vibration test to investigate the dynamic behavior of SPSP foundation during liquefaction. Based on the results, there are main findings as follows:

1) The ESA using both the Multi-spring and Cocktail glass model has almost the same trend as the dynamic responses in the vibration test. The difference in dynamic response of the foundation, superstructure, and ground between the flat and the slope models is minimal in the low-amplitude input ground motion, indicating that the effect of the ground slope is not significant. In cases of higher amplitude when liquefaction is observed, the effect of the ground slope becomes more significant, with the following trends: the slope causes an increase in the maximum displacements of the pile cap and superstructure. Furthermore, the slope causes an increase the maximum value of the bending and axial strain in the foundation pile. Therefore, the lateral movement of liquefaction layer due to the slope may partially affect the foundation during liquefaction.

2) The ESA using the multi-spring model can explain the behavior of the foundation with regard to maximum displacements, EPWP ratios, and bending strains during liquefaction. However, the calculated values of the residual displacement, etc. did not display a good agreement with the values observed in the vibration test.

3) The cocktail glass model that considers the dilative component of the sand and seepage of water can be used to estimate the dissipation of the pore water pressure. However, the response displacement using the cocktail glass model is smaller than that using the multi-spring model. The cocktail model could explain the dissipation of the pore water pressure in the vibration test; however, the calculation result had the vibration component and was not stable. Methods for determining the parameters in the ESA using both the multi-spring model and the cocktail glass model to correlate the test results should be examined in future studies.

## REFERENCES


1) Pile Damage Investigation Committee: Report of damage to building foundation during Hyogoken-Nanbu earthquake, Kinki Branch of AIJ, 399p, 1996.
2) Matsui, T., Kitazawa, M., Nanjo, A. and Yasuda, F.: Investigation of damaged foundations in the Great Hanshin earthquake disaster, *Seismic Behavior of Ground and Geotechnical Structures*, Secoe Pinto (ed.), Balkema, Rotterdam, pp.235-242, Geotechnical Engineering (KIG - Forum 97), Kansai Branch, Japanese Geotechnical Society, Osaka, Japan, 1997.
3) Ramin , M., Towhata, I., Honda, T., Tabata, K. and Abe, A.: Pile group response to liquefaction-induced lateral spreading: E-Defense large shake table test, *Journal Soil Dynamics and Earthquake Engineering*, Vol. 51, pp.35-46, 2013.
4) Tokida, K., Matsumota, H. and Iwasaki, H.: Experimental study on drag acting on piles in ground flowing by soil liquefaction, *Proc. 4th US-Japan Workshop on Earthquake Resistant Design of Lifeline Facilities and Countermeasures for Soil Liquefaction*, NCEER report 92- 0019, SUNY, Buffalo, pp.511-523, 1992.
5) Tokimatsu, K., Suzuki, H. and Sato, M.: Influence of inertial and Kinematic components on pile response during earthquakes, *Proc. 11th International Conference on Soil Dynamics and Earthquake Engineering*, pp.768-775, 2004.
6) JRA: Specifications for highway bridges, Japan Road Association, Preliminary English Version, prepared by Public Works Research Institute (PWRI) and Civil Engineering Research Laboratory (CRL), Japan, November 2002.
7) Iai, S.: Similitude for Shaking Table Tests on Soil-Structure Model in 1G Gravitational Field, *Report of the Port and Harbor Res. Inst.*, Vol.27, No.3, pp.3-24, 1988.
8) Iai, S.: A strain space multi mechanism model for cyclic behavior of sand and its application, *Report of Earthquake Engineering Research*, Note No.43, 1991.
9) Iai, S., Tobita, T., Ozutsumi, O. and Ueda, K.: Dilatancy of granular materials in a strain space multiple mechanism model, *International Journal for Numerical and Analytical Methods in Geomechanics*, Vol. 35, pp.360-390, 2011.
10) Ozutsumi, O.: Study on numerical analysis method of earthquake damage prediction for ground-structure system on liquefied layer, *doctoral dissertation, Kyoto university*, Dec.2003 (in Japanese).
11) Chapuis, R. P. and Aubertin, M.: Predicting the coefficient of permeability of soil using Kozeny-Carman equation, *Technical report*, EPM-RT-2003-3, 2003.